Frozen light in periodic stacks of anisotropic layers

J. Ballato
Center for Optical Materials Science and Engineering Technologies (COMSET), School of Materials Science and Engineering, Clemson University, Clemson, South Carolina 29634-0971, USA

A. Ballato
US Army Communications, Electronics Research, Development, and Engineering Center (CERDEC), Fort Monmouth, New Jersey 07703-5201, USA

A. Figotin and I. Vitebskiy
Department of Mathematics, University of California at Irvine, Irvine, California, 92697, USA
(Received 30 September 2004; published 18 March 2005)

We consider a plane electromagnetic wave incident on a periodic stack of dielectric layers. One of the alternating layers has an anisotropic refractive index with an oblique orientation of the principal axis relative to the normal to the layers. It was shown recently that an obliquely incident light, upon entering such a periodic stack, can be converted into an abnormal *axially frozen mode* with drastically enhanced amplitude and zero normal component of the group velocity. The stack reflectivity at this point can be very low, implying nearly total conversion of the incident light into the frozen mode with huge energy density, compared to that of the incident light. Supposedly, the frozen mode regime requires strong birefringence in the anisotropic layers—by an order of magnitude stronger than that available in common anisotropic dielectric materials. In this paper we show how to overcome the above problem by exploiting higher frequency bands of the photonic spectrum. We prove that a robust frozen mode regime at optical wavelengths can be realized in stacks composed of common anisotropic materials, such as YVO_4, $LiNbO_3$, $CaCO_3$, and the like.

DOI: 10.1103/PhysRevE.71.036612 PACS number(s): 42.70.Qs

I. INTRODUCTION

In photonic crystals, the speed of light is defined as the wave group velocity $\vec{u}$,

$$\vec{u} = \partial\omega/\partial\vec{k}, \tag{1}$$

where $\vec{k}$ is the Bloch wave vector and $\omega = \omega(\vec{k})$ is the corresponding frequency. At certain frequencies, the dispersion relation $\omega(\vec{k})$ of a photonic crystal develops stationary points

$$\partial\omega/\partial\vec{k} = 0, \tag{2}$$

in the vicinity of which the group velocity vanishes. Zero group velocity usually implies that the corresponding Bloch eigenmode does not transfer electromagnetic energy. Indeed, with certain reservations, the energy flux $\vec{S}$ of a Bloch mode is

$$\vec{S} = W\vec{u} \tag{3}$$

where W is the electromagnetic energy density, associated with this mode. If W is limited, then the group velocity $\vec{u}$ and the energy flux $\vec{S}$ vanish simultaneously at any stationary point (2) of the dispersion relation. Such modes are commonly referred to as slow modes, or slow light. Examples of different stationary points (2) are shown in Fig. 1, where each of the respective frequencies ω_a, ω_b, ω_g, and ω_0 is associated with slow light.

A common problem with slow modes is that most of them cannot be excited in semi-infinite photonic crystals by incident light. Indeed, consider a plane monochromatic wave incident on a semi-infinite photonic crystal with the electromagnetic dispersion relation shown in Fig. 1. If the frequency ω is close to the band edge frequency ω_g in Fig. 1, then the incident wave will be totally reflected back into space, as seen in Fig. 2.

In another case, where the incident wave frequency is close to the characteristic value ω_a or ω_b in Fig. 1, some portion of the incident wave will be transmitted in the photonic crystal, but none in the form of the slow mode corresponding to the respective stationary point. This means, for example, that at the frequency ω_a, the transmitted light is a Bloch wave with finite group velocity and wave number different from that corresponding to the point *a* in Fig. 1.

Let us turn now to the stationary inflection point 0 of the dispersion relation in Fig. 1, where both the first and the second derivatives of the frequency ω with respect to k vanish, while the third derivative is finite,

$$\frac{\partial\omega}{\partial k} = 0, \quad \frac{\partial^2\omega}{\partial k^2} = 0, \quad \frac{\partial^3\omega}{\partial k^3} \neq 0 \quad \text{at } \omega = \omega_0 \text{ and } k = k_0. \tag{4}$$

The frequency ω_0 of stationary inflection point is associated with the so-called *frozen mode regime* [1–3]. In such a case, the incident plane wave can be transmitted into the photonic crystal with little reflection, as seen in Fig. 2. Having entered the photonic slab, the light is 100% converted into the slow mode with infinitesimal group velocity and drastically enhanced amplitude. Under the frozen mode regime, vanishingly small group velocity $\vec{u}$ in Eq. (3) is offset by a huge

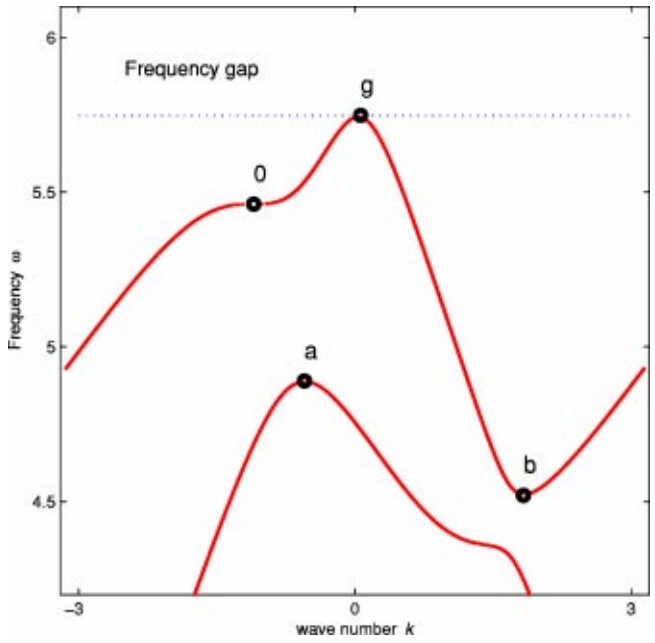

FIG. 1. (Color online). An example of electromagnetic dispersion relation $\omega(k)$ with various stationary points: (i) extreme points a and b of the respective spectral branches, (ii) a photonic band edge g, (iii) a stationary inflection point 0. Each stationary point is associated with slow light. The wave number k and the frequency ω are given in units of $1/L$ and c/L, respectively. L is the primitive translation of the periodic array.

value of the energy density W. As a result, the energy flux (3) associated with the frozen mode remains finite and comparable with that of the incident wave. In the vicinity of the frozen mode frequency ω_0, the electromagnetic energy density W associated with the slow (frozen) mode displays a resonancelike behavior,

$$W \approx \frac{2\tau S_I}{6^{2/3}}(\omega_0''')^{-1/3}(\omega-\omega_0)^{-2/3}, \tag{5}$$

where S_I is the fixed energy flux of the incident wave, τ is the portion of the incident light transmitted into the semi-infinite photonic crystal, and

$$\omega_0''' = \left(\frac{\partial^3\omega}{\partial k^3}\right)_{k=k_0}.$$

Remarkably, the transmittance τ at $\omega \approx \omega_0$ remains finite and may even be close to unity, as shown in Fig. 2. The latter implies that a significant portion of the incident light is converted into the frozen mode with nearly zero group velocity and huge amplitude, compared to that of the incident wave. In reality, the electromagnetic energy density W of the frozen mode will be limited by such factors as absorption, nonlinear effects, imperfection of the periodic dielectric array, deviation of the incident radiation from a perfect plane monochromatic wave, finiteness of the photonic slab dimensions, etc. Still, with all these limitations in place, the frozen mode regime can be very attractive for various practical applications.

From now on we restrict ourselves to the case of lossless periodic layered media (periodic stacks), which can be viewed as one-dimensional photonic crystals. According to [2], at normal incidence, the frozen mode regime in a periodic stack can occur only if some of the layers display sufficiently strong circular birefringence (Faraday rotation). In addition, each unit cell of the periodic layered array must contain at least two layers with significant and misaligned in-plane anisotropy. If the above conditions are not met, the electromagnetic dispersion relation of the periodic stack cannot develop a stationary inflection point (4) and, therefore, cannot support the frozen mode regime at normal incidence. In the microwave frequency range, one can find a number of

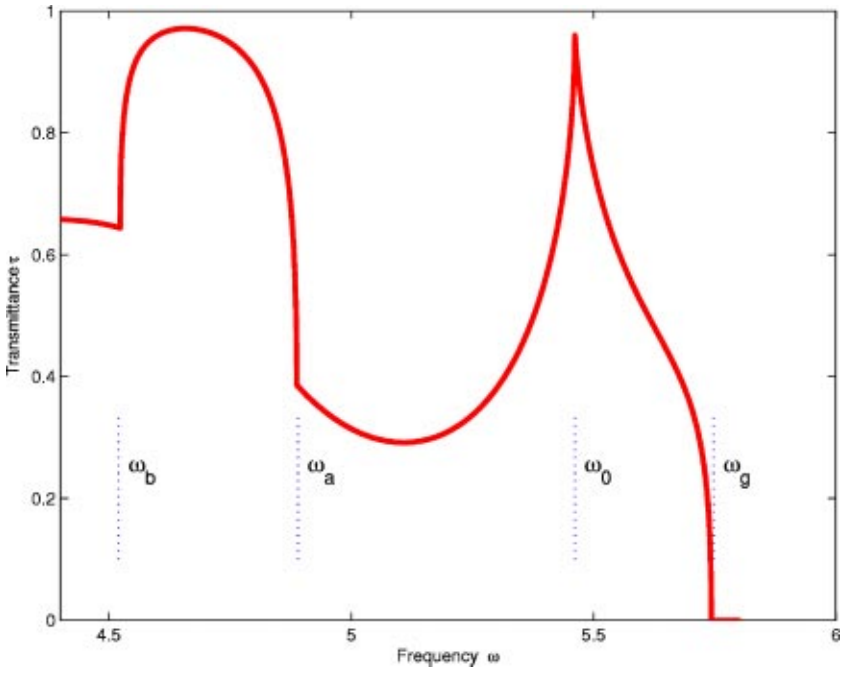

FIG. 2. (Color online). Transmittance τ as a function of incident light frequency ω for the semi-infinite photonic slab with the dispersion relation presented in Fig. 1. The characteristic frequencies ω_a, ω_b, ω_0, and ω_g are associated with the respective stationary points in Fig. 1. At $\omega \geqslant \omega_g$ (within the photonic band gap) the incident light is totally reflected by the slab. Frequency ω is expressed in units of c/L.

materials meeting the above requirements. But at infrared and optical frequencies, the circular birefringence of known transparent magnetic materials becomes too small to support a robust frozen mode regime [2]. Since our prime interest here is with optics, we will explore the "nonmagnetic" approach proposed in [3].

According to [3], the frozen mode regime can occur in nonmagnetic periodic stacks with special configurations requiring some layers to display appreciable oblique (neither in-plane nor axial) anisotropy. On the other hand, at optical frequencies, all commercially available anisotropic dielectrics display substantially weaker anisotropy, compared to what would be the optimal value. According to [3], too weak anisotropy can push the frozen mode frequency too close to the nearest band edge, resulting in almost total reflectance of the incident light. The high reflectance of the slab, in turn, implies very low efficiency of conversion of the incident light into the slow mode. In this paper we show that in fact the negative effect of the weak anisotropy on the frozen mode regime can be completely overcome by proper design of the layered structure. As the result, a robust frozen mode regime at optical frequencies can be achieved in periodic stacks incorporating real anisotropic materials such as yttrium vanadate, lithium niobate, and the like, where the dielectric anisotropy is one or two orders of magnitude short of the "optimal" value. The idea is to choose the parameters of the periodic stack so that a stationary inflection point associated with the frozen mode regime develops at higher photonic bands. For a given frequency range, this requires thicker dielectric layers, which could be an additional practical advantage. A side effect of using higher photonic bands is that the effective bandwidth of the frozen mode regime appears to be narrower, compared to the case of hypothetical materials with much stronger anisotropy used in [3] for numerical simulations.

The practical development of frozen mode devices from such commodity materials could lead to revolutionary advances in optical computing, sensing, and information processing. When practically realized, such frozen mode structures would enable significant advances in all-optical information storage and processing (such as optical memory and buffer elements, optical delay lines) as well as optical sensing, lasing, and nonlinear optics.

The paper is organized as follows. In the next section, we discuss in general terms the phenomenon of axially frozen mode. The detailed analysis of the mathematical aspects of the phenomenon can be found in [3]. Then, in Sec. III, using a specific example of a periodic array incorporating yttrium vanadate, we demonstrate how a robust frozen mode regime at optical frequencies can be achieved in a practical setting involving weakly anisotropic materials. Finally, in the Appendix, we briefly overview the electrodynamics of lossless layered media, introducing basic notations, definitions, and assumptions used in our computations.

II. AXIALLY FROZEN MODE REGIME AT OBLIQUE INCIDENCE

According to [2,3], in nonmagnetic periodic stacks, the simplest version of the frozen mode regime described in the Introduction is impossible. Still, a more general phenomenon referred to as the *axially frozen mode regime* can occur. This section starts with a brief general discussion of the phenomenon. Then we turn to the particular case of a periodic stack incorporating yttrium vanadate layers. The reason we have chosen this particular material is because its optical properties are very similar to those of other common anisotropic dielectrics transparent at optical wavelengths.

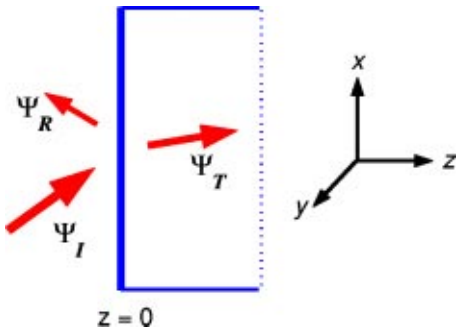

FIG. 3. (Color online). Light incident on a semi-infinite photonic slab. The arrows show the energy fluxes of the incident, reflected, and transmitted waves, respectively. The transmitted wave Ψ_T is a superposition of two Bloch eigenmodes, each of which can be either propagating or evanescent. Only propagating modes can transfer electromagnetic energy in the z direction.

A. Basic definitions

Consider a monochromatic plane wave obliquely incident on a periodic semi-infinite stack, as shown in Fig. 3. The plane $z=0$ coincides with the slab/vacuum interface.

Let Ψ_I, Ψ_R, and Ψ_T denote the incident, reflected, and transmitted waves, respectively. Due to the boundary conditions (A12), all three waves Ψ_I, Ψ_R, and Ψ_T must be assigned the same pair of tangential components k_x, k_y of the corresponding wave vector [4–6]

$$(\vec{k}_I)_x = (\vec{k}_R)_x = (\vec{k}_T)_x, \quad (\vec{k}_I)_y = (\vec{k}_R)_y = (\vec{k}_T)_y, \tag{6}$$

while their axial (normal) components k_z can be different. Hereinafter, the symbol k_z will refer only to the transmitted Bloch waves propagating inside the semi-infinite slab

$$\vec{k} = (k_x, k_y, k_z) \quad \text{inside periodic stack (at } z > 0). \tag{7}$$

The value k_z is defined up to a multiple of $2\pi/L$ (the Brillouin zone), where L is the period of the layered structure. For given k_x, k_y, and ω, the value k_z is found by solving the time-harmonic Maxwell equations (A3) in a periodic medium, which will be done in the following sections. The result can be represented as the axial *dispersion relation*, which gives the correspondence between ω and k_z at fixed k_x, k_y,

$$\omega = \omega(k_z) \text{ at fixed } k_x, k_y. \tag{8}$$

It can be more convenient to define the axial dispersion relation as the correspondence between ω and k_z at fixed direction $\vec{n}$ of incident light propagation,

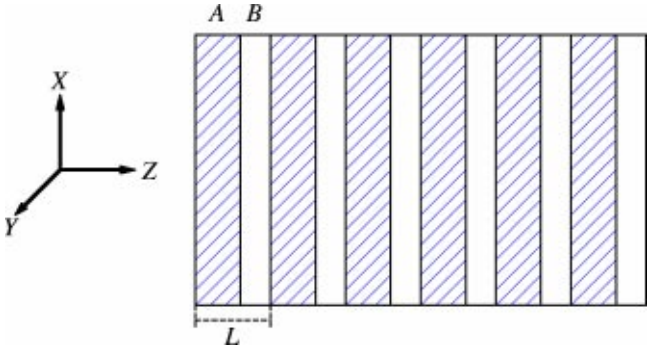

FIG. 4. (Color online). Periodic array of anisotropic dielectric layers (A) separated by gaps (B). The anisotropy axis of the dielectric material (the tetragonal axis, in the case of yttrium vanadate) makes an oblique angle with the z direction, normal to the layers. The stack parameters used in our numerical simulations are specified in formulas (30) and (31).

$$\omega = \omega(k_z) \text{ at fixed } n_x, n_y, \tag{9}$$

where the unit vector $\vec{n}$ can be expressed in terms of the tangential components (6) of the wave vector

$$n_x = k_x c/\omega,\ n_y = k_y c/\omega,\ n_z = \sqrt{1-(n_x^2+n_y^2)}. \tag{10}$$

Examples of the axial dispersion relation (9) are presented in Figs. 5 and 6. Small gaps appearing near the stationary points of the spectral branches are numerical artifacts.

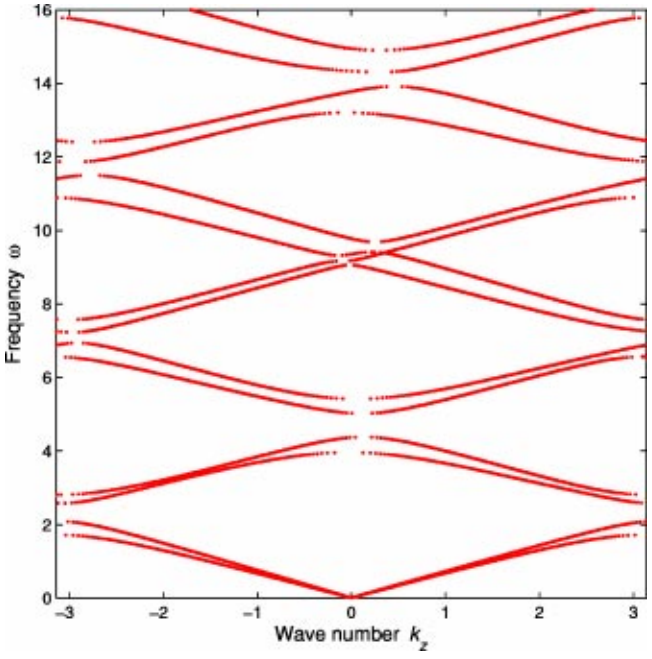

FIG. 5. (Color online). The axial dispersion relation $\omega(k_z)$ of the periodic stack in Fig. 4 at fixed direction $\vec{n}$ of light incidence ($n_x = n_y = -0.493\,489$). The small spectral asymmetry and small branch separation are due to the weak anisotropy of yttrium vanadate. Both the asymmetry and the branch separation are more prononced in upper spectral bands. The wave number k_z and the frequency ω are given in units of $1/L$ and c/L, respectively.

The transmitted electromagnetic field Ψ_T inside the periodic layered medium is not a single Bloch mode, but it is a superposition of two Bloch modes with different polarizations and different values of k_z. Of course, the tangential components k_x, k_y are the same for either transmitted Bloch mode and the incident wave, as stated by Eq. (6). Generally, there are three possibilities (see the details in [3]).

(1) Both Bloch components of the transmitted wave Ψ_T are propagating modes, which means that the corresponding values of k_z are real. For example, at $\omega < \omega_a$ and $\omega > \omega_b$ in Fig. 6 we have two Bloch modes propagating inside the slab with two different group velocities $u_z > 0$ (double refraction). Note that propagating modes with $u_z < 0$, as well as evanescent modes with $\mathrm{Im}(k_z) < 0$, do not contribute to the transmitted wave Ψ_T inside the semi-infinite stack in Fig. 3.

(2) Both Bloch components of Ψ_T are evanescent, which implies that the corresponding values of k_z are complex with $\mathrm{Im}(k_z) > 0$. In particular, this is the case if the frequency ω falls into a photonic band gap (for example, at $\omega > \omega_g$ in Fig. 1). In such a case, the incident wave is totally reflected back to space.

(3) Of particular interest is the case when one of the Bloch components of the transmitted wave Ψ_T is a propagating mode (with $u_z > 0$), while the other is an evanescent mode (with $\mathrm{Im}(k_z) > 0$)

$$\Psi_T = \Psi_{pr} + \Psi_{ev}. \tag{11}$$

This is the case at the frequency range

$$\omega_a < \omega < \omega_b \tag{12}$$

in Fig. 6. As the distance z from the slab/vacuum interface increases, the evanescent contribution Ψ_{ev} decays as $\exp[-z\,\mathrm{Im}(k_z)]$, and the resulting transmitted wave Ψ_T turns into a single propagating Bloch eigenmode Ψ_{pr}.

Similarly to the case (4) of a regular frozen mode, the *axially frozen mode* is associated with the *axial stationary inflection point* defined as

$$\frac{\partial \omega}{\partial k_z} = 0, \frac{\partial^2 \omega}{\partial k_z^2} = 0, \frac{\partial^3 \omega}{\partial k_z^3} \neq 0 \quad \text{at } \omega = \omega_0. \tag{13}$$

The regular stationary inflection point (4) is a particular case of (13). An example of an axial dispersion relation displaying such a singularity is shown in Fig. 6. In the vicinity of ω_0 in Eq. (13), the electromagnetic field Ψ_T inside the slab is a superposition (11) of one propagating and one evanescent Bloch component. As the frequency ω approaches the critical point (13), both contributions grow sharply, while remaining nearly equal and opposite in sign near the slab boundary (at $z=0$), as illustrated in Fig. 7.

Due to the destructive interference at the slab boundary, the resulting electromagnetic field at $z=0$ is small enough to satisfy the boundary condition (A12). As the distance z from the slab boundary increases, the evanescent component Ψ_{ev} decays exponentially, while the amplitude of the propagating component Ψ_{pr} remains constant and large, as shown in Figs. 8(b) and 8(c).

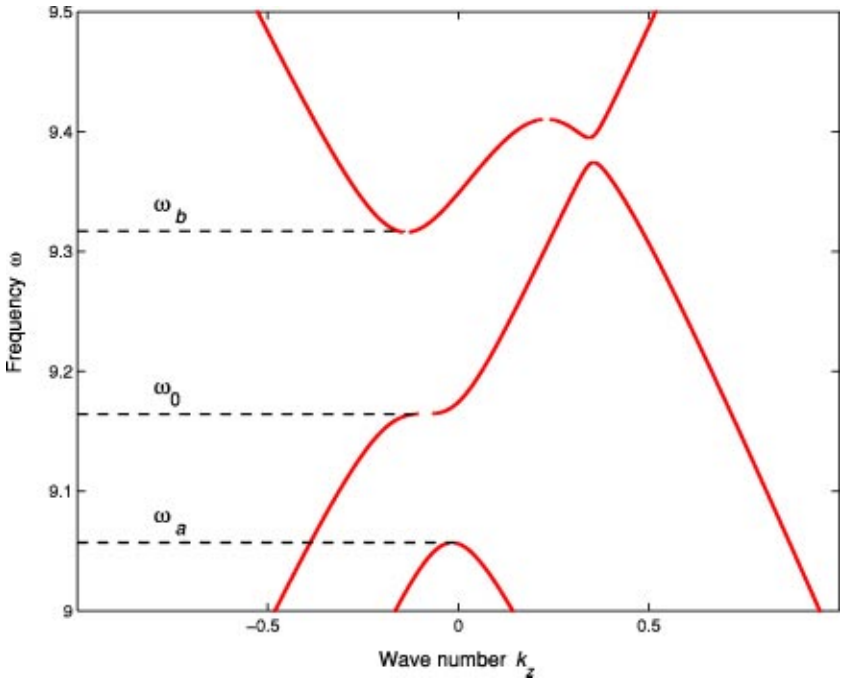

FIG. 6. (Color online). A fragment of the axial dispersion relation $\omega(k_z)$ in Fig. 5, which includes the axial stationary inflection point at $\omega_0 = 9.164\,450\,223$. Small discontinuities appearing near stationary points of the spectral branches are numerical artifacts.

B. Energy density and energy flux of the axially frozen mode

Let $\vec{S}_I$, $\vec{S}_R$, and $\vec{S}_T$ be the energy fluxes of the incident, reflected, and transmitted waves, respectively. Within the frequency range (12), which includes the critical point (13), the transmitted wave Ψ_T is a superposition (11) of propagating and evanescent components. Only the propagating component Ψ_{pr} is responsible for the axial energy flux $(\vec{S}_T)_z$.

The axial energy flux can also be expressed in terms of the axial component u_z of the propagating mode group velocity and the energy density W_0 associated with Ψ_{pr}

$$(\vec{S}_T)_z = W_0 u_z \propto |\Psi_{pr}|^2 u_z. \tag{14}$$

The quantity W_0 in Eq. (14) can be interpreted as the electromagnetic energy density far from the slab interface, where the electromagnetic field Ψ_T reduces to its propagating component Ψ_{pr}. In the vicinity of the axial stationary inflection point (13), the energy density W_0, associated with the axially frozen mode, diverges, while $u_z \to 0$. As a result, the vanishingly small u_z in Eq. (14) is offset by a very large value of W_0. The theoretical analysis of the next section shows that the axial energy flux $(\vec{S}_T)_z$ in Eq. (14), along with the slab transmittance τ in Eq. (A20), remain finite even at $\omega = \omega_0$, where the axial component of the group velocity vanishes,

$$(\vec{S}_T)_z > 0 \quad \text{if } u_z = 0. \tag{15}$$

The energy conservation consideration allows us to find the asymptotic frequency dependence of the amplitude $|\Psi_{pr}|^2$ of the axially frozen mode in the vicinity of the critical point (13). Indeed, in the vicinity of ω_0, the axial dispersion rela-

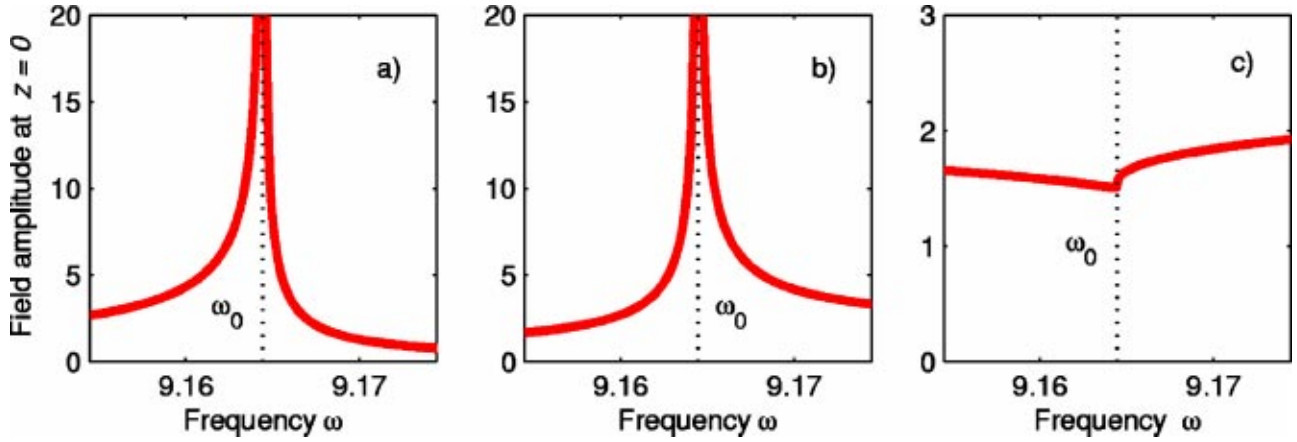

FIG. 7. (Color online). Destructive interference of the propagating and evanescent contributions to the resulting field Ψ_T at the slab/vacuum interface under the frozen mode regime: (a) amplitude $|\Psi_{pr}(0)|^2$ of the propagating component, (b) amplitude $|\Psi_{ev}(0)|^2$ of the evanescent component, and (c) resulting field amplitude $|\Psi_T(0)|^2$. Frequency ω is expressed in units of c/L. The incident light has unit amplitude and TE polarization.

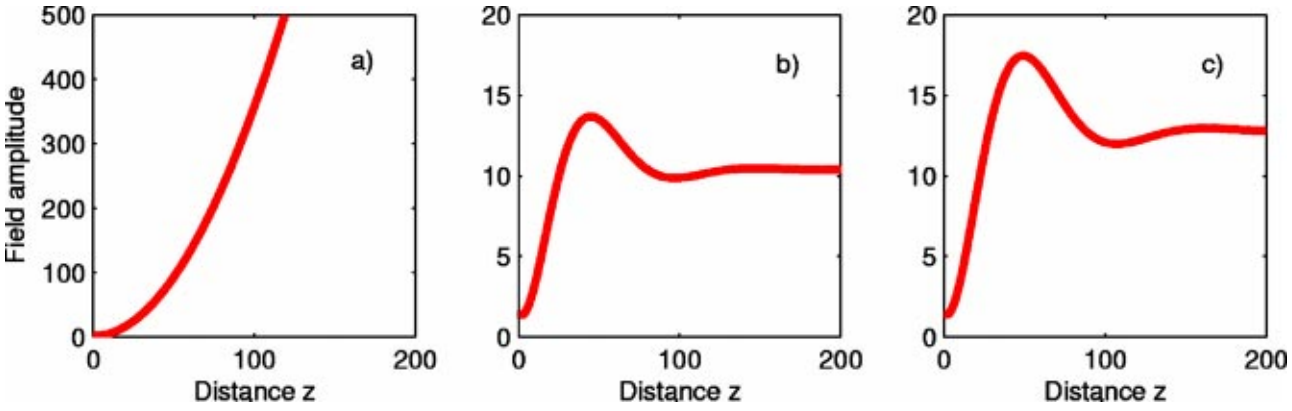

FIG. 8. (Color online). The amplitude $|\Psi(z)|^2$ of the resulting field as a function of the distance z from the slab boundary: (a) $\omega=\omega_0$, $n=n_0$, which is the exact point of the frozen mode regime; (b) $\omega\neq\omega_0$, $n=n_0$, the frequency ω deviates from ω_0 by $10^{-3}c/L$; (c) $\omega=\omega_0$, $n\neq n_0$, the direction n of light incidence deviates from n_0 in Eq. (33) by 10^{-4}. The distance z is given in units of L. The incident light has unit amplitude and TE polarization.

tion can be approximated by a cubic parabola

$$\omega-\omega_0\approx\frac{1}{6}\omega_0'''(k_z-k_0)^3,\quad \omega_0'''=\left(\frac{\partial^3\omega}{\partial k_z^3}\right)_{\vec{k}=\vec{k}_0}. \tag{16}$$

The z component of the group velocity is

$$u_z=\frac{\partial\omega}{\partial k_z}\approx\frac{1}{2}\omega_0'''(k_z-k_0)^2\approx\frac{6^{2/3}}{2}(\omega_0''')^{1/3}(\omega-\omega_0)^{2/3}. \tag{17}$$

Equation (17) together with Eq. (14) yield the following asymptotic expression for the energy density W_0 associated with the frozen mode:

$$W_0\approx\frac{2}{6^{2/3}}(\vec{S}_T)_z(\omega_0''')^{-1/3}(\omega-\omega_0)^{-2/3}, \tag{18}$$

or, equivalently,

$$W_0\approx\frac{2}{6^{2/3}}\tau(\vec{S}_I)_z(\omega_0''')^{-1/3}(\omega-\omega_0)^{-2/3}, \tag{19}$$

where $\vec{S}_I$ is the fixed energy flux of the incident wave and τ is the transmittance coefficient defined in Eq. (A20). Remarkably, the transmittance τ of the semi-infinite slab remains finite in the vicinity of the frozen mode frequency ω_0, as seen in Figs. 9 and 10. This implies that the electromagnetic energy density W_0 associated with the frozen mode, as well as its amplitude $|\Psi_{pr}|^2$, diverge as $\omega\to\omega_0$. In Figs. 9 and 10 such a behavior is illustrated for two different incident light polarizations.

In reality, under the axial frozen mode regime, the field amplitude inside the slab is limited by various physical factors mentioned earlier in this paper. Still, with all these limitations in place, the normal energy flux $(\vec{S}_T)_z$ remains finite and comparable with that of the incident wave. The latter implies that a substantial portion of the incident wave is converted into the axially frozen mode with drastically enhanced amplitude and nearly zero axial component u_z of the group velocity. In many respects, the phenomenon of axial frozen mode is similar to its particular case, the regular frozen mode, associated with the regular stationary inflection point (4).

C. Physical conditions for the axially frozen mode regime in layered media

The physical conditions under which a nonmagnetic layered structure can support the (axial) frozen mode regime can be grouped in two categories. The first one comprises several symmetry restrictions. The second category includes some basic qualitative recommendations which would ensure the robustness of the frozen mode regime, provided that the symmetry conditions for the regime are met. In what follows we briefly reiterate those conditions and then show how they apply to periodic stacks incorporating some real dielectric materials.

1. Symmetry conditions

There are two fundamental necessary conditions for the frozen mode regime. The first one is that the Bloch dispersion relation $\omega(\vec{k})$ in the periodic layered medium must display the so-called *axial spectral asymmetry*

$$\omega(k_x,k_y,k_z)\neq\omega(k_x,k_y,-k_z). \tag{20}$$

As shown in [3], this condition is necessary for the existence of the axial stationary inflection point (13) in the electromagnetic dispersion relation of an arbitrary periodic layered medium.

The second necessary condition is that for the given direction $\vec{k}$ of wave propagation, the Bloch eigenmodes $\Psi_{\vec{k}}$ with different polarizations must have the same symmetry. In the case of oblique propagation in periodic layered media, the latter condition implies that for the given $\vec{k}$, the Bloch eigenmodes are neither TE nor TM,

$$\Psi_{\vec{k}}\text{ is neither TE nor TM}. \tag{21}$$

The condition (20) imposes certain restrictions on (i) the point symmetry group G of the periodic layered array and (ii) the direction $\vec{k}$ of the transmitted wave propagation inside

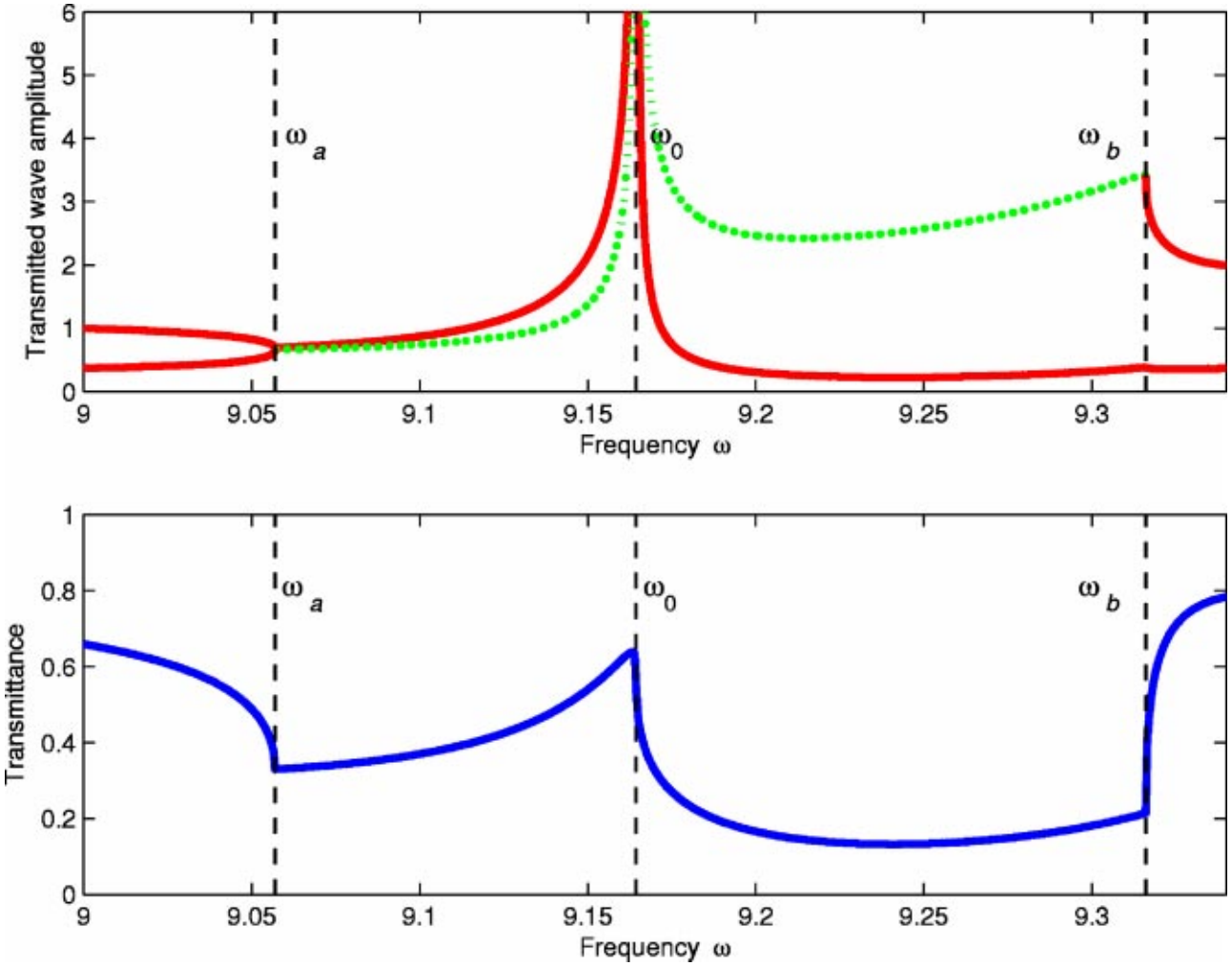

FIG. 9. (Color online). At the top: the solid (red) line shows the amplitude $|\Psi_{pr}|^2$ of the propagating Bloch component of the transmitted wave Ψ_T from Eq. (11). The dotted (green) line shows the amplitude $|\Psi_{ev}|^2$ of the evanescent component. Both contributions to Ψ_T diverge at the frozen mode frequency ω_0. At $z \gg L$, the evanescent component decays and $|\Psi_{pr}|^2$ (the solid line) represents the resulting amplitude $|\Psi_T|^2$ of the transmitted wave. By contrast, at $\omega < \omega_a$ and $\omega > \omega_b$, the transmitted wave Ψ_T is a superposition of two propagating components (double refraction). At the bottom: the slab transmittance τ vs frequency ω. At $\omega = \omega_0$, the transmittance remains finite. The characteristic frequencies ω_a, ω_0, and ω_b are explained in Fig. 6. The incident wave has TE polarization and unit amplitude. Frequency ω is given in units of c/L.

the layered medium. The condition (21) may impose some additional restriction on the direction of $\vec{k}$.

The restriction on the symmetry of the periodic stack following from the requirement (20) of axial spectral asymmetry is

$$m_z \notin G \text{ and } 2_z \notin G, \tag{22}$$

where m_z is the mirror plane parallel to the layers and 2_z is the twofold rotation about the z axis. An immediate consequence of the criterion (22) is that at least one of the alternating layers of the periodic stack must be an anisotropic dielectric material with nonzero ε_{xz} and/or ε_{yz}, where the z direction is normal to the layers,

$$\varepsilon_{xz} \neq 0 \text{ and/or } \varepsilon_{yz} \neq 0. \tag{23}$$

Otherwise, the operation 2_z will be present in the symmetry group G of the periodic stack.

The condition (20) also imposes a restriction on the direction of wave propagation. Specifically, the Bloch wave vector $\vec{k}$ must be oblique to the stack layers, which means that $\vec{k}$ is neither parallel nor perpendicular to the z direction,

$$k_x \neq 0 \text{ and/or } k_y \neq 0.$$

The latter condition implies that the frozen mode regime cannot occur at normal incidence, regardless of the periodic stack geometry and composition. While the condition (23) implies that at least one of the alternating layers must be cut at an oblique angle relative to the principal axes of its permittivity tensor. If either of the above two conditions is not satisfied, the dispersion relation $\omega(\vec{k})$ will be axially symmetric

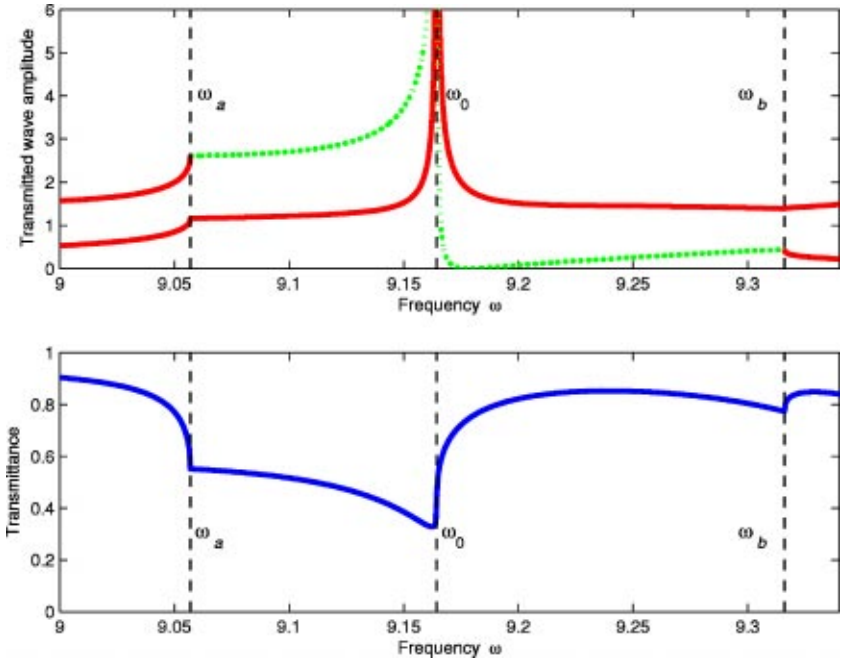

FIG. 10. (Color online). The same as in Fig. 9, but the incident wave polarization is now TH.

$$\omega(k_x,k_y,k_z) = \omega(k_x,k_y,-k_z), \tag{24}$$

which rules out the possibility of a stationary inflection point and the frozen mode regime.

If all the above necessary conditions are met, then the (axial) frozen mode regime is, at least, not forbidden by symmetry. More details on the symmetry aspects of the frozen mode regime can be found in [3], Sec. II, and [2], Secs. I and II.

2. Additional physical requirements

In practice, as soon as the symmetry conditions are met, one can almost certainly achieve the (axial) frozen mode regime at any desirable frequency ω within a certain frequency range. The frequency range is determined by the layer thicknesses and the dielectric materials used, while a specific value of ω within the range can be selected by the direction $\vec{n}$ of the light incidence. The problem is that unless the physical parameters of the stack layers lie within a certain range, the effects associated with the frozen mode regime can be insignificant or even practically undetectable. The basic guiding principle in choosing appropriate layer materials is "moderation." As soon as the "moderation" principle is observed, one can almost certainly achieve the frozen mode regime at prescribed frequency by choosing the right direction of light incidence. Specifically, those "moderation" conditions include the following.

(1) It is desirable that the ratio

$$\frac{\Delta n}{n} \tag{25}$$

of the birefringence and the refractive index of the material of the anisotropic layers lies somewhere between 2 and 10. If the anisotropy is extremely strong or too weak, the Bloch waves with different polarizations become virtually separated, which excludes the possibility of a robust frozen mode regime. For example, in the practically important case of extremely small anisotropy, the two transmitted Bloch waves can be approximately classified as TE and TM modes, which is incompatible with the symmetry condition (21) for the frozen mode regime.

(2) The dielectric contrast of the adjacent layers A and B should be significant, but not extreme. The ratio n_A/n_B anywhere between 1.5 and 20 would be appropriate. In addition, the dielectric contrast between the layers should match the ratio (25) in the anisotropic layers: weaker anisotropy would require weaker dielectric contrast between the layers.

(3) Typical layer thickness should be of the order of $\lambda/4n$, where $\lambda = 2\pi/\omega$ is the light wavelength in vacuum and n is the corresponding refractive index. In reality, the acceptable layer thickness can differ from $\lambda/4n$ by several times either way. But too thick layers would push the stationary inflection point to high order frequency bands, while too thin layers would exclude the possibility of the frozen mode regime at the prescribed frequency range.

The biggest challenge at optical frequencies poses the first condition, because most of the commercially available optical anisotropic crystals have the ratio $\Delta n/n$ of only about 0.1. According to [3], this would push the axial stationary inflection point (13) very close to the photonic band edge and make the photonic crystal almost 100% reflective. This indeed would be the case if we tried to realize the frozen mode regime at the lowest frequency band. But, in the next section we show that one can successfully solve this problem by moving to a higher frequency band. So a robust axially frozen mode regime with almost complete conversion of the incident light into the frozen mode can be achieved with commercially available anisotropic dielectric materials displaying a birefringence ratio (25) smaller by one on two orders of magnitude, compared to the optimal value used in [3] for numerical simulations. The drawback though is that using higher photonic frequency bands narrows the bandwidth of the frozen mode regime by roughly an order of magnitude.

III. PERIODIC STACK INCORPORATING YTTRIUM VANADATE LAYERS

The simplest nonmagnetic periodic stack satisfying the symmetry conditions (22) and (23) and, therefore, capable of supporting the axial frozen mode regime, is shown in Fig. 4. It is composed of anisotropic A layers separated by empty gaps. The anisotropic dielectric layers must display nonzero components ε_{xz} and/or ε_{yz}. The simplest choice for the corresponding permittivity tensor is

$$\hat{\varepsilon}_A = \begin{bmatrix} \varepsilon_{xx} & 0 & \varepsilon_{xz} \\ 0 & \varepsilon_{yy} & 0 \\ \varepsilon_{xz} & 0 & \varepsilon_{zz} \end{bmatrix} \tag{26}$$

where the z axis coincides with the normal to the layers.

Yttrium vanadate is a tetragonal dielectric with the permittivity tensor $\hat{\varepsilon}_{YV}$ at $\lambda = 1550$ nm [7]

$$\hat{\varepsilon}_{YV} = \begin{bmatrix} \varepsilon_{11} & 0 & 0 \\ 0 & \varepsilon_{22} & 0 \\ 0 & 0 & \varepsilon_{33} \end{bmatrix} = \begin{bmatrix} 4.62 & 0 & 0 \\ 0 & 4.62 & 0 \\ 0 & 0 & 3.78 \end{bmatrix} \tag{27}$$

where the Cartesian axis x_3 is chosen parallel to the crystallographic axis C_4. In order to achieve a nonzero ε_{xz} component one has to rotate the tensor (27) about the y axis by an angle θ different from 0 and $\pi/2$ [8]. The result of the rotation is

$$\hat{\varepsilon}_A = \begin{bmatrix} \varepsilon_{11}\cos^2\theta + \varepsilon_{33}\sin^2\theta & 0 & (\varepsilon_{11} - \varepsilon_{33})\cos\theta\sin\theta \\ 0 & \varepsilon_{22} & 0 \\ (\varepsilon_{11} - \varepsilon_{33})\cos\theta\sin\theta & 0 & \varepsilon_{33}\cos^2\theta + \varepsilon_{11}\sin^2\theta \end{bmatrix}. \tag{28}$$

For numerical simulations we can choose, for instance,

$$\theta = \pi/4. \tag{29}$$

In this case, Eq. (28) together with (27) yields

$$\hat{\varepsilon}_A = \begin{bmatrix} 4.20 & 0 & 4.42 \\ 0 & 4.62 & 0 \\ 4.42 & 0 & 4.20 \end{bmatrix} \tag{30}$$

which is compatible with the required form (26).

Let d_A and d_B denote the thickness of the A layers and the thickness of the gaps between them, respectively. For our numerical simulations we can choose

$$d_A = d_B = L/2, \tag{31}$$

where L is the period of the layered array in Fig. 4.

Let us reiterate that the parameters (29) and (31) are chosen at random. In practice, we can always adjust them so that the stack suits specific practical requirements. The structural period L should be chosen so that the frozen mode regime occurs within a prescribed frequency range. Then, the direction of light incidence can be adjusted so that the axial frozen mode regime occurs exactly at a prescribed frequency ω_0.

Symmetry arguments similar to those presented in [3] show that in the case of the periodic array in Fig. 4, the necessary conditions (22) and (21) for the frozen mode regime are satisfied only if the direction $\vec{n}$ of the light incidence lies in neither the x-z nor the y-z plane,

$$n_x \neq 0 \text{ and } n_y \neq 0. \tag{32}$$

A. Electromagnetic properties in the vicinity of axial frozen mode regime

In Fig. 5 we presented the typical axial dispersion relation $\omega(k_z)$ of the periodic stack in Fig. 4 at fixed direction $\vec{n}$ of light incidence. In Fig. 5 we chose

$$n_x = n_y = n_0 \quad \text{where } n_0 = -0.493\,489, \tag{33}$$

because this particular direction of light incidence produces the axially frozen mode regime at certain frequency ω_0, shown in Fig. 6. Due to the relatively small anisotropy of yttrium vanadate, the axial dispersion relation in Fig. 5 displays rather weak asymmetry $\omega(k_z) \neq \omega(-k_z)$, which makes it virtually impossible to develop a stationary inflection point at the lowest spectral branches. As we go to upper photonic bands, the situation improves. In Fig. 6 we present the enlarged fragment of the axial dispersion relation in Fig. 5. This fragment covers the boundary region between the forth and the fifth bands. At frequency

$$\omega_0 = 9.164\,450\,223c/L \tag{34}$$

one of the spectral branches develops axial stationary inflection point (13), associated with the possibility of the axial frozen mode regime.

Our numerical analysis based on the transfer matrix approach (the computational details are presented in the Appendix) indeed shows a very robust (axial) frozen mode regime in this setting, in spite of the fact that the dielectric anisotropy of yttrium vanadate is more than an order of magnitude short of the optimal value. The drawback though is that the frequency bandwidth of the effect is roughly an order of magnitude narrower, compared to what could be achieved with hypothetical materials displaying much stronger anisotropy at optical frequencies.

Let us start with the results presented in Figs. 9 and 10. The bottom plots in both figures display the frequency dependence of the stack transmittance τ for two different polarizations of incident light. Clearly, in the vicinity of the frozen mode frequency ω_0, the transmittance remains significant, which implies that a significant portion of the incident radiation is converted into the frozen mode. The top plots in Figs. 9 and 10 display the amplitudes of the two Bloch components of the transmitted wave Ψ_T. The solid and dotted lines correspond to the propagating and evanescent Bloch components, respectively. In the vicinity of the frozen mode frequency (at $\omega_a < \omega < \omega_b$), there is one propagating component (Ψ_{pr}) and one evanescent component (Ψ_{ev}), each of which diverges as $\omega \to \omega_0$, in accordance with Eq. (19). At $\omega < \omega_a$ and $\omega > \omega_b$, the transmitted wave Ψ_T is a superposition of two propagating components with different group velocities, which constitutes the phenomenon of double refraction. The characteristic frequencies in Figs. 9 and 10 are explained in Fig. 6.

Figure 7 shows the frequency dependence of the resulting field amplitude $|\Psi_T(0)|^2$ at the slab boundary, along with the

amplitudes of its propagating and evanescent components $|\Psi_{pr}(0)|^2$ and $|\Psi_{ev}(0)|^2$. Although each of the two Bloch contributions to $\Psi_T(0)$ diverges as $\omega \to \omega_0$, their superposition $\Psi_T(0)$ remains finite, to meet the boundary conditions (A12) at $z=0$. As we move further away from the slab boundary, the evanescent component dies out, while the propagating mode $\Psi_{pr}(z)$ remains constant and large. As a result, the destructive interference of $\Psi_{pr}(z)$ and $\Psi_{ev}(z)$ is removed, and the resulting field amplitude $|\Psi_T(z)|^2$ grows and approaches the value $|\Psi_{pr}|^2$. This scenario is illustrated in Figs. 8(b) and 8(c). If the frequency ω of the incident wave and its direction of propagation $\vec{n}$ exactly correspond to the critical values ω_0 and $\vec{n}_0$, then the electromagnetic field $\Psi_T(z)$ inside the semi-infinite stack is described by a linearly diverging non-Bloch Floquet eigenmode

$$|\Psi_T|^2 \propto z^2,$$

as shown in Fig. 8(a).

By way of example, let us present the actual geometrical parameters of the stack supporting the axially frozen mode regime for the case of infrared light with $\lambda = 1550$ nm and the direction of incidence (33). The expression (34) for the frozen mode frequency yields

$$d = L/2 = 1130.4 \text{ nm}.$$

In practice, we do not have to adjust the layer thicknesses in order to achieve the frozen mode regime at a prescribed wavelength. Instead, we can tune the system into the axially frozen mode regime by adjusting the direction $\vec{n}$ of light incidence.

IV. CONCLUSIONS

The most important conclusion of our analysis is that a robust frozen mode regime can be realized in periodic stacks incorporating generic anisotropic dielectric materials, such as YVO_4, $LiNbO_3$, and $CaCO_3$, where the anisotropy of the refractive index is well below the optimal value. At optical frequencies, periodic dielectric arrays can reduce the speed of pulse propagation by roughly three orders of magnitude. This is not a fundamental physical limitation, but rather a technological restriction related to the difficulty of building flawless periodic arrays at nanoscales. Due to almost complete and lossless conversion of the incident light into the slow frozen mode, such a slowdown implies the enhancement of the electromagnetic energy density in the slow mode by the same three orders of magnitude. This can be very attractive for a variety of practical applications.

Relatively weak anisotropy of generic dielectric materials imposes more severe bandwidth limitations on the frozen mode regime, but this can only affect the cases involving ultrashort light pulses. Otherwise, all the major manifestations of the frozen mode regime, such as the dramatic increase of the frozen light amplitude compared to that of the incident light, remain in place.

ACKNOWLEDGMENTS

The effort of A.F. and I.V. was supported by the U.S. Air Force Office of Scientific Research under Grant No. FA9550-04-1-0359. J.B. also wish to thank the Defense Advanced Research Projects Agency (DARPA) for support under Grant No. N66001-03-1-8900 through SPAWAR.

APPENDIX: SCATTERING PROBLEM FOR ANISOTROPIC SEMI-INFINITE STACK

In this appendix we briefly discuss the standard procedure we use to do the electrodynamics of stratified media incorporating anisotropic layers. For more details, see, for example, [3,9–11] and references therein.

1. Time-harmonic Maxwell equations in periodic layered media

Our consideration is based on time-harmonic Maxwell equations

$$\nabla \times \mathbf{E}(x,y,z) = i\frac{\omega}{c}\mathbf{B}(x,y,z),$$

$$\nabla \times \mathbf{H}(x,y,z) = -i\frac{\omega}{c}\mathbf{D}(x,y,z) \tag{A1}$$

with linear constitutive relations

$$\mathbf{D}(x,y,z) = \hat{\varepsilon}(z)\mathbf{E}(x,y,z), \quad \mathbf{B}(x,y,z) = \hat{\mu}(z)\mathbf{H}(x,y,z). \tag{A2}$$

In layered media, the tensors $\hat{\varepsilon}$ and $\hat{\mu}$ in Eq. (A2) depend on a single Cartesian coordinate z. Plugging Eq. (A2) into (A1) yields

$$\nabla \times \mathbf{E}(x,y,z) = i\frac{\omega}{c}\hat{\mu}(z)\mathbf{H}(x,y,z),$$

$$\nabla \times \mathbf{H}(x,y,z) = -i\frac{\omega}{c}\hat{\varepsilon}(z)\mathbf{E}(x,y,z). \tag{A3}$$

Solutions for Eq. (A3) are sought in the following form:

$$\mathbf{E}(x,y,z) = e^{i(k_x x + k_y y)}\vec{E}(z), \quad \mathbf{H}(x,y,z) = e^{i(k_x x + k_y y)}\vec{H}(z), \tag{A4}$$

which is a standard choice for the scattering problem of a plane electromagnetic wave incident on a plane-parallel stratified slab. Indeed, in such a case, due to the boundary conditions (A11), the tangential components (k_x, k_y) of the wave vector are the same for the incident, reflected, and transmitted waves. The substitution (A4) in Eq. (A3) allows one to separate the tangential field components E_x, E_y, H_x, H_y into a closed system of four linear differential equations,

$$\partial_z \Psi(z) = i\frac{\omega}{c}M(z)\Psi(z) \quad \text{where } \Psi(z) = \begin{bmatrix} E_x(z) \\ E_y(z) \\ H_x(z) \\ H_y(z) \end{bmatrix}. \tag{A5}$$

The 4×4 matrix $M(z)$ is referred to as the Maxwell operator. The reduced Maxwell equation (A5) for the four tangential

field components $\Psi(z)$ should be complemented with the following expressions for the normal components of the fields:

$$E_z = (-n_x H_y + n_y H_x - \varepsilon^*_{xz} E_x - \varepsilon^*_{yz} E_y)\varepsilon^{-1}_{zz},$$

$$H_z = (n_x E_y - n_y E_x - \mu^*_{xz} H_x - \mu^*_{yz} H_y)\mu^{-1}_{zz}, \quad \text{(A6)}$$

where

$$n_x = ck_x/\omega, \quad n_y = ck_y/\omega. \quad \text{(A7)}$$

The expression for the Maxwell operator $M(z)$ is very cumbersome; its explicit form can be found in [3]. The matrix elements of $M(z)$ depend on the following parameters: the frequency ω, the direction $\vec{n}$ of light incidence, and the material tensors $\hat{\varepsilon}(z)$ and $\hat{\mu}(z)$.

In a periodic layered medium

$$M(z+L) = M(z), \quad \text{(A8)}$$

where L is the stack period. For any given k_x, k_y, and ω, the system (A5) of four ordinary linear differential equations with periodic coefficients has four Bloch solutions,

$$\Psi_{k_i}(z+L) = e^{ik_i L}\Psi_{k_i}(z), \; i = 1,2,3,4, \quad \text{(A9)}$$

where k_i, $i=1,2,3,4$, correspond to four solutions for k_z for given k_x, k_y, and ω,

$$k_x, k_y, \omega \leftrightarrow \{k_{1z}, k_{2z}, k_{3z}, k_{4z}\} = \{k^*_{1z}, k^*_{2z}, k^*_{3z}, k^*_{4z}\}. \quad \text{(A10)}$$

Real k_z in Eq. (A10) relate to propagating Bloch eigenmodes, while complex k_z relate to the evanescent modes. In the case of propagating eigenmodes, the correspondence between k_z and ω for fixed k_x, k_y is referred to as the axial dispersion relation, the concise form of which is given by Eq. (8) or (9).

The reduced Maxwell equations (A5) in periodic layered media are analyzed and solved using the transfer matrix formalism, the detailed description of which can be found in the extensive literature on the subject (see, for example, [3,9–11] and references therein).

2. Boundary conditions

The boundary conditions at the slab/vacuum interface reduce to the continuity requirement for the tangential field components at $z=0$,

$$[\mathbf{E}_I(x,y,0)]_\perp + [\mathbf{E}_R(x,y,0)]_\perp = [\mathbf{E}_T(x,y,0)]_\perp,$$

$$[\mathbf{H}_I(x,y,0)]_\perp + [\mathbf{H}_R(x,y,0)]_\perp = [\mathbf{H}_T(x,y,0)]_\perp, \quad \text{(A11)}$$

where the indices I, R, and T denote the incident, reflected, and transmitted waves, respectively. Using representation (A4), we can recast (A11) in a compact form

$$\Psi_I(0) + \Psi_R(0) = \Psi_T(0) \quad \text{(A12)}$$

where

$$\Psi_I = \begin{bmatrix} E_{I,x} \\ E_{I,y} \\ H_{I,x} \\ H_{I,y} \end{bmatrix} = \begin{bmatrix} E_{I,x} \\ E_{I,y} \\ -E_{I,x} n_x n_y n_z^{-1} - E_{I,y}(1-n_x^2)n_z^{-1} \\ E_{I,x}(1-n_y^2)n_z^{-1} + E_{I,y} n_x n_y n_z^{-1} \end{bmatrix}, \quad \text{(A13)}$$

$$\Psi_R = \begin{bmatrix} E_{R,x} \\ E_{R,y} \\ H_{R,x} \\ H_{R,y} \end{bmatrix} = \begin{bmatrix} E_{R,x} \\ E_{R,y} \\ E_{R,x} n_x n_y n_z^{-1} + E_{R,y}(1-n_x^2)n_z^{-1} \\ -E_{R,x}(1-n_y^2)n_z^{-1} - E_{R,y} n_x n_y n_z^{-1} \end{bmatrix}$$

describe the incident and reflected waves, respectively. n_x, n_y, and n_z are the Cartesian components of the unit vector (10).

Knowing the eigenmodes (A9) inside the slab and using the boundary conditions (A12) we can express the amplitude and composition of the transmitted wave Ψ_T and reflected wave Ψ_R in terms of the amplitude and polarization of the incident wave Ψ_I. This gives us the electromagnetic field distribution $\Psi_T(z)$ inside the layered medium, as well as the transmittance and reflectance coefficients of the semi-infinite slab as functions of the incident wave polarization, the direction $\vec{n}$ of incidence, and the frequency ω.

3. Energy flux, reflectance, transmittance

The real-valued Poynting vector is defined by

$$\vec{S}(x,y,z) = \frac{1}{2}\,\mathrm{Re}[\mathbf{E}^*(x,y,z) \times \mathbf{H}(x,y,z)]. \quad \text{(A14)}$$

Plugging the representation (A4) for $\mathbf{E}(x,y,z)$ and $\mathbf{H}(x,y,z)$ in Eq. (A14) yields

$$\vec{S}(x,y,z) = \vec{S}(z) = \frac{1}{2}\,\mathrm{Re}[\vec{E}^*(z) \times \vec{H}(z)], \quad \text{(A15)}$$

implying that none of the three Cartesian components of the energy density flux $\vec{S}$ depends on the tangential coordinates x and y. In addition, the energy conservation argument implies that the axial component S_z of the energy flux does not depend on the coordinate z either,

$$S_z(x,y,z) = S_z = \text{const}, \quad S_x(x,y,z) = S_x(z), \quad S_y(x,y,z) = S_y(z). \quad \text{(A16)}$$

This applies only to the case of a plane monochromatic wave incident on a lossless layered medium. The explicit expression for the z component of the energy flux (A15) is

$$S_z = \frac{1}{2}[E^*_x H_y - E^*_y H_x + E_x H^*_y - E_y H^*_x]. \quad \text{(A17)}$$

Let us turn to the scattering problem for a semi-infinite slab. Let $\vec{S}_I$, $\vec{S}_R$, and $\vec{S}_T$ be the Poynting vectors of the incident, reflected, and transmitted waves, respectively. Energy conservation imposes the following relation between the normal components of these three vectors:

$$(\vec{S}_T)_z = (\vec{S}_I)_z + (\vec{S}_R)_z. \quad \text{(A18)}$$

Since the stack is presumably composed of lossless materials, the z component of the energy flux is independent of coordinates both inside and outside the stack. In particular, inside the slab we have

$$(\vec{S}_T)_z = \text{const.} \quad \text{at } z > 0. \tag{A19}$$

The transmittance (τ) and the reflectance (ρ) of a lossless semi-infinite slab are defined as

$$\tau = \frac{(\vec{S}_T)_z}{(\vec{S}_I)_z}, \quad \rho = -\frac{(\vec{S}_R)_z}{(\vec{S}_I)_z} = 1 - \tau. \tag{A20}$$

[1] A. Figotin and I. Vitebsky, Phys. Rev. E **63**, 066609 (2001).
[2] A. Figotin and I. Vitebskiy, Phys. Rev. B **67**, 165210 (2003).
[3] A. Figotin and I. Vitebskiy, Phys. Rev. E **68**, 036609 (2003).
[4] L. D. Landau, E. M. Lifshitz, and L. P. Pitaevskii, *Electrodynamics of Continuous Media* (Pergamon, New York, 1984).
[5] Amnon Yariv and Pochi Yeh, *Optical Waves in Crystals* (Wiley, New York, 1984).
[6] Pochi Yeh, *Optical Waves in Layered Media* (Wiley, New York, 1988).
[7] *Smithsonian Physical Tables*, 9th rev. ed., edited by W. Forsythe (Knovel Publishing, Danbury, CT, 2003).
[8] J. Ballato and A. Ballato, (unpublished).
[9] D. W. Berreman, J. Opt. Soc. Am. A **62**, 502 (1972).
[10] I. Abdulhalim, J. Opt. A, Pure Appl. Opt. **1**, 646 (1999).
[11] I. Abdulhalim, J. Opt. A, Pure Appl. Opt. **2**, 557 (2000).